Applied Thermal Engineering 236 (2024) 121915

Contents lists available at ScienceDirect

Applied Thermal Engineering

journal homepage: www.elsevier.com/locate/apthermeng

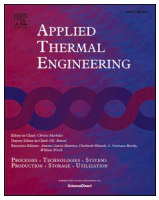

Research Paper

Numerical investigation of a district scale groundwater heat pump system: A case study from Colchester, UK

Taha Sezer [a,*], Abubakar Kawuwa Sani [a], Rao Martand Singh [b], Liang Cui [a], David P. Boon [c], Michael Woods [d]

[a] University of Surrey, Civil and Environmental Engineering, Guildford GU2 7XH, UK
[b] Department of Civil & Environmental Engineering, Norwegian University of Science & Technology (NTNU), Trondheim 7034, Norway
[c] British Geological Survey, Keyworth, Nottingham NG12 5GG, UK
[d] Colchester Amphora Energy Ltd, Rowan House, 33 Sheepen Road, Colchester CO3 3WG, UK

ARTICLE INFO

Keywords:
Renewable energy
District heating
Groundwater heat pump
Chalk aquifer
Thermally affected zone
FEFLOW

ABSTRACT

Nearly 40% of Europe's total energy consumption is dedicated to buildings and heating/cooling make a significant part of this consumption. Groundwater heat pumps (GWHP) are highly efficient, and low-carbon technology that can supply heating/cooling to buildings on small or large scales. Thus, they contribute to achieving European targets of net-zero greenhouse gas emissions by 2050. In the literature, studies on the utilisation of GWHP at a district scale, particularly in chalk aquifers, are relatively rare. The implementation of district-scale geothermal heat pump (GWHP) systems poses several challenges, including dealing with the scale and complexity of the systems, addressing geological variability, managing high initial investments, balancing energy demand and supply, ensuring proper maintenance and monitoring, and mitigating potential environmental impacts. These challenges require careful consideration and strategic planning to ensure the successful deployment and sustainable operation of these systems., This study numerically investigates a district-scale GWHP system and analyses the thermal plume development created due to the heating operation, offering insights into system performance. A good match was found between field results and simulation results for water level increase and drawdown. However, there is a difference of approximately 11% in system efficiency between field tests and simulations due to the lower abstraction temperature detected in the simulation. The simulation results show that cooler water injection into the fractured chalk aquifer creates a thermal plume radially spanning out to 50 m. The thermal plume has no effect on the abstraction temperature and system performance. This result can be attributed to the large distance between injection and abstraction wells and the low hydraulic gradient.

1. Introduction

Combating climate change and ensuring energy security requires the development of alternative energy supplies such as wind, biomass, solar, wave and geothermal energy other than fossil fuels. In Europe, buildings (residential and non-residential) are responsible for 40% of total energy consumption [1]. A significant part of this consumption comes from heating/cooling; and generally, fossil fuels are used in meeting the energy demand at small/single building unit to a large scale district level. The latter is often termed as district heating and cooling (DHC) technology.

The advancement of the technology to 5th generation DHC ensures the system operates at low temperature, making it more energy efficient, with lower heat losses and achieving more cost savings [2]. The DHC technology can integrate and use various energy sources including waste heat, local fuels or renewables (e.g. groundwater heat pump (GWHP)) for energy generation.

GWHP system is a technology that uses groundwater source (at depths > 500 m or shallower) to supply heating and cooling energy need of buildings, with high coefficient of performance (COP) [3]. A higher system performance can be achieved by coupling the GWHP and DHC technology, and particularly when interseasonal loads are balanced, making it a highly efficient low-carbon heating/cooling system [4]. However, environmental or system sustainability issues such as thermal interference, changes in water chemistry, mobilisation of contaminants

* Corresponding author.
E-mail address: t.sezer@surrey.ac.uk (T. Sezer).

https://doi.org/10.1016/j.applthermaleng.2023.121915
Received 4 July 2023; Received in revised form 16 October 2023; Accepted 2 November 2023
Available online 4 November 2023
1359-4311/© 2023 The Author(s). Published by Elsevier Ltd. This is an open access article under the CC BY license (http://creativecommons.org/licenses/by/4.0/).

Nomenclatures

BH1	Borehole 1
BH2	Borehole 2
BH3	Borehole 3
BH4	Borehole 4
BH5	Borehole 5
COP	Coefficient of performance
DHC	District heating and cooling
GSHP	Ground source heat pump
GWHP	Groundwater heat pump
m bgl	Meter below ground level
m aOD	Meter above ordnance datum

and saline water, and changes to groundwater levels around abstraction and injection wells need to be considered in design [3].

It is generally preferred to reinject the extracted water back into the same aquifer to maintain a stable pressure head. This operation creates a change in the groundwater temperature (called thermal plume), which can reach the abstraction well, thereby affecting the extracted water temperature. This phenomenon is called thermal feedback when the injection temperature is constant, or thermal recycling when the difference between injection and abstraction temperature is constant [5].

The occurrence of thermal feedback in GWHPs primarily depends on the distance between wells, abstraction and injection rate (thermal load of the building), groundwater flow velocity (hydraulic gradient), the aquifer size and the injection temperature [7]. Recent studies have focused on analysing the environmental impact of GWHP utilisation and evaluating the development of the thermally affected zone (TAZ) around injection wells, which can affect the thermal sustainability of the system [8–15]. They reported that time-dependent numerical modelling approach can predict TAZ development around injection wells. Additionally, they emphasise the significance of carefully considering the risk of thermal feedback during GWHP system design.

Several studies have been conducted investigating the thermal plume development around wells. Russo et al. [16] and Russo and Civita [17] reported that the thermal plume developed around wells depend on factors including groundwater reinjection rate and higher temperature changes in the heat exchanger resulting from greater energy demand.

Herbert et al. [18] carried out a study on an existing aquifer scale open loop system in London. The results indicated a reduced efficiency of the system in densely populated areas of London due to thermal interference. Gropius [19] carried out a numerical groundwater flow and heat transport modelling for GWHP systems in the London chalk aquifer. He suggested that while GSHPs are a viable choice for accomplishing renewable energy goals, it is crucial to exercise cautious risk management as inadequately designed or situated schemes may not yield the desired performance. Birks et al. [20] conducted a case study considering a GSHP system fed by groundwater extracted from a chalk aquifer. They emphasised that the performance of individual boreholes and their interaction directly influences the effectiveness of the GWHP system in heating and cooling applications. Additionally, other studies by Arthur et al. [21] and Headon et al. [22] reported the performance of the chalk aquifer in the UK, specifically focusing on its hydraulic and thermal characteristics.

In addition, some of the key challenges that limit the installation of GWHP systems have been reported by many researchers, and it include intricate coordination among multiple wells, extensive piping networks, substantial initial investments required, and complex heat exchange systems [23,24]. Similarly, other environmental issues that impacts on the system performance which still needs to be further understood are geological variability, groundwater flow patterns, thermal characteristics of the aquifer, and the maximum allowable changes to ground temperature, and the thermal interaction between boreholes.

Thus, this paper presents a numerical study investigating the thermal effects of district-scale (greater than 800 kW) GWHP operation on the environment. The paper aims to predict the maximum temperature magnitude developed in the chalk aquifer and the temperature interactions between boreholes over a continuous operation. Furthermore, the paper provides insights into system performance and aquifer impacts. Thermal plume development around a set of injection wells was modelled to evaluate far-field effects considering a proposed district-scale heating system in a chalk aquifer in the UK.

2. Case study

2.1. Site description

The case study, called Colchester Northern Gateway Heat Network, is an ongoing project located in the town of Colchester, UK (see Fig. 1). The planned project will probably be the largest GWHP system using the confined chalk aquifer to date in the UK. It will provide district heating and domestic hot water (DHW) to healthcare buildings, around 300 dwellings, and offices [25]. The site elevation is around 48 m aOD (meter above ordnance datum). The annual mean average air temperature in Colchester is 9.9 °C, and the mean air temperatures for the hottest and coldest days are 22 °C and 2 °C, respectively [26].

The system is designed as part-load to cover 75% of the annual heating demand of the planned development with an 800 kW output heat pump which will extract thermal energy from groundwater extracted using two wells equipped with submersible pumps set at a depth of around 110 m. Gas boilers are also installed at the site to cover the rest of the demand, particularly peak loads in winter and can be used as a backup system. The abstracted ambient groundwater temperature is between 12 °C and 13 °C, which is then transferred to the centralised high-temperature heat pump, where it is amplified to approximately 65 °C to meet the heating and hot water demands of the buildings.

The temperature of groundwater exiting the heat exchangers will be around 5 °C, and the groundwater will be injected into three wells located more than 530 m away from the two abstraction wells. Borehole locations are shown in Fig. 2. Table 1 gives information about steel casing, open hole length, temperature and water level measured during the investigation in injection wells including Borehole 1 (BH1), Borehole 2 (BH2) and Borehole 3 (BH3), and abstraction wells Borehole 4 (BH4) and Borehole 5 (BH5). Lessons learned from the groundwater investigation, well development and test pumping stages are reported by Birks et al. [20] who reiterate the need for reverse circulation drilling methods and acidisation to develop chalk wells prior to pump tests and operation.

The geological sequence at Colchester Northern Gateway is given in Table 2. The sequence is fairly typical of the London Basin and comprises of topsoil/made ground, thin sands and gravels, London Clay, Lambeth Group (with Thanet), and chalk. The Cretaceous chalk aquifer lies from around 73 to 275 m bgl (meters below ground level) and overlies the Cretaceous Gault Clay [29]. A Cretaceous chalk aquifer is an underground geological formation primarily consisting of chalk rock from the Cretaceous period (between 145 million and 66 million years ago). Chalk in this area is a soft, white, highly porous limestone rock composed of calcite shells from microscopic marine organisms. These aquifers represent subsurface layers of chalk rock often containing abundant supplies of groundwater are these groundwater bodies are therefore legally protected in the UK requiring permits to abstract greater than 20 m3/day or inject waste or thermally-spent water.

The conceptual hydrogeological model of the site, shown in Fig. 3, depicts the main geological formations, groundwater flow direction, abstraction and injection well locations, design pumping rates and primary temperatures. With the injection wells positioned up groundwater gradient from the abstraction wells and potential karstic development, there is a risk of thermal plume migration towards the abstraction wells and reduction in abstracted water temperature over time. This is a key

Fig. 1. Location of the study area [27].

Fig. 2. Borehole locations [27].

risk for GWHPs, as described by Birks et al. [32]. This paper assesses this risk by employing a numerical heat flow modelling approach.

Fig. 4 shows the working principle of the heat pump system, with the primary heat source being groundwater from the chalk aquifer. The groundwater is conveyed from the chalk aquifer to the evaporator, where it transfers its heat to the refrigerant. As a result, the refrigerant

Table 1
Borehole construction data with observed rest water levels in the chalk [28].

Borehole number	Steel casing (m bgl)	Steel casing diameter (m)	Open hole (m bgl)	Open hole diameter (m)	Water level (m bgl)	Water level (m aOD)
1	0–75.96	0.345	75.9–135	0.3	45.6	2.4
2	0–75.96		75.96–200		45.7	2.3
3	0–76.5		76.5–137		44.9	3.1
4	0–77		77–200		46.5	1.5
5	0–77.4		77.4–135		47.2	0.8

Table 2
Geological sequence at Colchester Northern Gateway (modified after [20], adapted from [30]; following stratigraphic framework of [31].

	Geological Units	Depth to top of layer (m bgl)	Layer thickness (m)
Quaternary	Topsoil & Made Ground	0	1
	Coverloam & Kesgrave Sand & Gravel	1	5
Palaeogene	*Thames Group*		
	London Clay Formation – silty clay and claystone with rare sands and concretions of cementstone	6	36
	Harwich Formation – silty and sandy clays and minor silts, glauconitic	42	8
	Lambeth Group	50	10
	Clay, silt and sandy, with some sands and gravels, minor limestones and lignite, occasional sandstones and conglomerates		
	Thanet Formation*	60	12
	Fine sand, minor clay		
Cretaceous	*White Chalk Sub-Group***		202
	Newhaven Chalk Formation	72	23
	Soft marly chalk, non-flinty, karstified with open joints in upper part	95	59
	Seaford Chalk Formation		
	Chalk with hard flint nodules and bands including 'Seven Sisters	154	c.45
	Flint Band' Lewis Nodular Chalk Formation***	c.199	c.75
	Hard nodular chalk (Chalk Rock Mbr)		
	New Pit and Holywell Formations		
Lower Cretaceous	*Gray Chalk Subgroup* – chalk (undifferentiated)	c.275	c.45
	Gault Clay Formation – grey mudstone	c.320	6 to 23
Silurian	Shales and slates; folded and faulted	c.325–340	>100 *m*

* Secondary Aquifer, ** Principal Aquifer, *** c.31 m proved in BH2 and BH4 based on natural gamma logs and image log interpretation [20]. 'c.' indicates circa, where thicknesses in strata are uncertain due to a lack of deep borehole data.

begins to boil, becoming a low-pressure vapor. Subsequently, it is directed to the compressor, where the low-pressure refrigerant vapor is transformed into a high-pressure, high-temperature vapor. This high-temperature vapor then enters the condenser, where it transfers its thermal energy to a secondary circulation fluid, ultimately providing heat to the building(s). The entire system operates in a closed loop, allowing the refrigerant to return to the evaporator and continue the vapor compression cycle.

2.2. Pumping tests

Several pumping tests were carried out to confirm the sustainability of the planned project [20]. After installation of the boreholes, constant rate tests were carried out to gather crucial information about well characteristics, reservoir assessment and optimisation of well operation. Additionally, hydraulic balance tests were undertaken to assess the pressure within the geothermal reservoir, detect leaks or crossflow, and evaluate reservoir connectivity. All these tests are aimed at ensuring the sustainable management of geothermal resources for energy production. The step test was conducted by applying four different flow rates of 2, 4, 6 and 8 l/s in steps. In the constant rate test, the flow rate was kept constant at 7.5 l/s. The hydraulic balance test was carried out at two flow rates, starting at 6 l/s and then increasing to 8.5 l/s. In this test, the increase and decrease in water levels were recorded. Based on the conducted tests, it was determined that two wells (BH4 and BH5) situated on the eastern side of the site would serve as extraction wells, each with a maximum yield of 9 l/s (18 l/s combined), whilst three wells (BH1, BH2, and BH3) on the western side were designated as injection wells, each with a maximum injection rate of 6 l/s.

When developing a numerical model to examine hydraulic and thermal transport processes, it is important to consider the main geological controls and their influence on groundwater flow processes. In the case of this duel-porosity chalk aquifer, it was important to identify any changes in aquifer thickness between boreholes to assess the presence or absence of fractures and the extent of karstic development in the rock mass. Boon et al. [30] investigated the geological and hydrogeological characteristics of the five boreholes at CNG and the ground between them, utilising a combination of downhole geophysical and surface passive seismic methods. The study provided valuable insights that were integrated into the numerical model setup and sources of uncertainty, including depths of key lithostratigraphic formation boundaries, the groundwater table one year on after drilling and test pumping, casing depths and borehole wall condition, and undisturbed fluid temperature and conductivity profiles. They also observed an 18 m long vertical fracture (open joint) between 77 and 95 m bgl in BH4 entirely within the Newhaven Chalk Formation. Features such this open fracture are likely to provide a significant contribution to the yields obtained when pumping from a well, and if laterally extensive over hundreds of meters, pose a potential rapid transport pathway between injection and abstraction wells that could cause thermal short cut or thermal feedback. None of the other wells in CNG had open fractures (based on available optical image data), so discrete fractures were not added to the numerical model. Also, the geology layer were proved to be near-horizontal so dipping layers were not required in the model.

The average water level measured in the boreholes in Feb 2020 was 45.0 m bgl (approximately 3 m aOD) [30]. Fig. 5 shows the undisturbed groundwater temperature profiles at the site. Boon et al. [30] stated that the temperature gradient at the site is variable with depth, between 2 °C and 2.6 °C per 100 m, with the steepest gradient seen in the clay-rich Paleogene cover and the lowest gradient in the chalk between 100 and 200 m depth interval. Kicks detected in temperature log profiles in Fig. 5 are suggestive of local variations in the flow characteristics. The maximum and minimum groundwater temperatures measured by the British Geological Survey in 2020 were 10.16 °C at 45 m bgl and

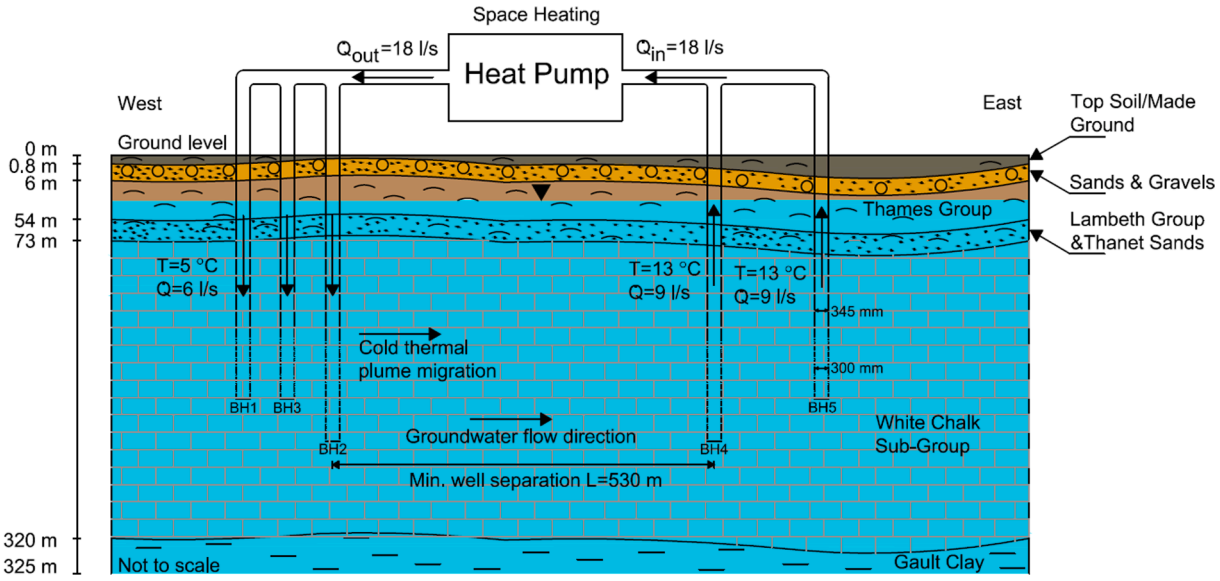

Fig. 3. The conceptual hydrogeological model including boreholes, maximum abstraction/injection rates and design abstraction and injection temperatures.

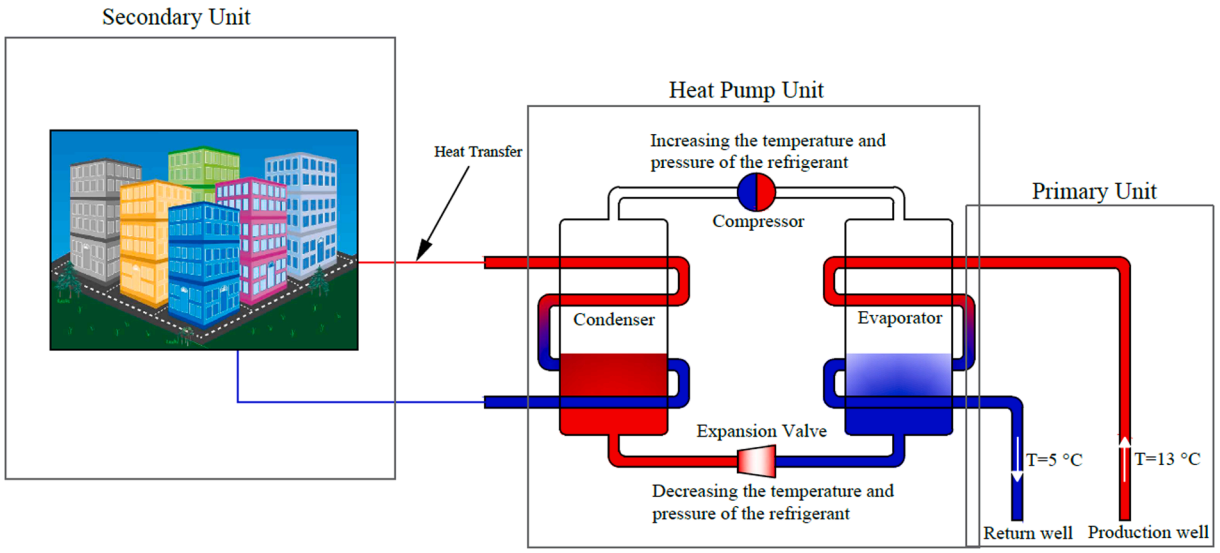

Fig. 4. Groundwater source heat pump working principle with temperature information from the case study (Modified from [6]).

14.18 °C at 200 m bgl. However, considering the submersible pump inlets in the abstraction wells are designed to be set at c.110 m bgl, the undisturbed pumped temperature range would likely be around 12.5 °C to 13.0 °C.

A recharge test was also performed from the abstraction wells to the injection wells [20] and the findings from these test was incorporated in the numerical model. The drawdown developed during the recharge test was monitored. The results showed that a significant drawdown was created due to the abstraction. The rest water level in the abstraction wells dropped by a maximum of 70 m when the abstraction rate was 9–10 l/s. The water level in the injection well rose up to the ground level. The pressure given during the test equals around 20 m water head; therefore, it was decided the injection well head must be sealed and pressurised up to 2 Bar to mitigate the risk of surface flooding [20]. After the pumping test, the recovery time of each well was recorded. After almost 1 day, the water level at the abstraction wells recovered back to the initial level. However, the recovery time of the injection wells was longer than that of the abstraction wells, which is around 10 days. This difference between the recovery times can be attributed to the fact that the soil around the injection wells are less productive than the abstraction wells (which benefited from being drilled with reverse circulation flush technique and received acidization treatments to develop), but this may improve over time as fines are flushed out of the fractures.

Fig. 6 shows the design monthly total heating demand, heat pump output, and thermal energy obtained from groundwater, assuming a heap pump COP of 3.91. In the project, the heat pump system covers 75% of the total thermal load of the buildings. As expected, the heating demand is higher in winter compared to the heating demand in summer. Therefore, variable injection and abstraction rates were applied in the simulation (see Fig. 7). The injection temperature was kept constant during the simulation.

The pumping tests showed that the maximum flow rate of abstraction wells is between 9 and 10 l/s. The current system is designed with a maximum abstraction rate of 9 l/s per borehole (BH4&5). The maximum injection rate was designed as 6 l/s for each reinjection well, considering the total abstraction and injection rate of 18 l/s.

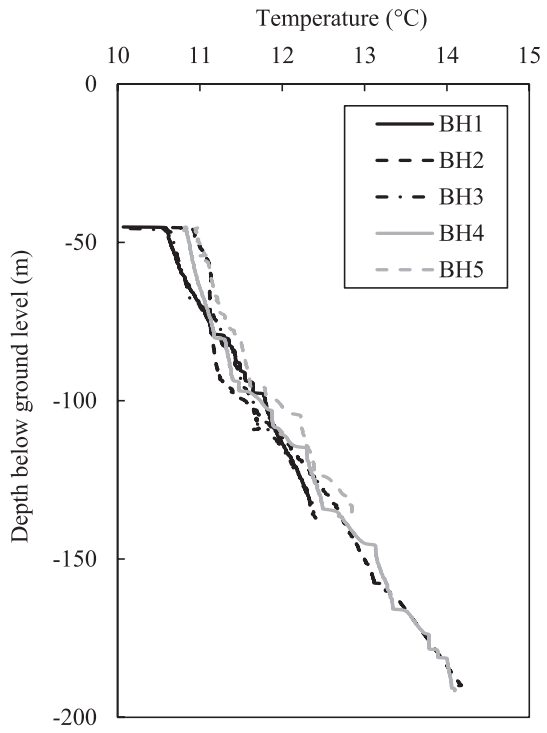

Fig. 5. Measured groundwater temperature profiles ().
adapted from [30]

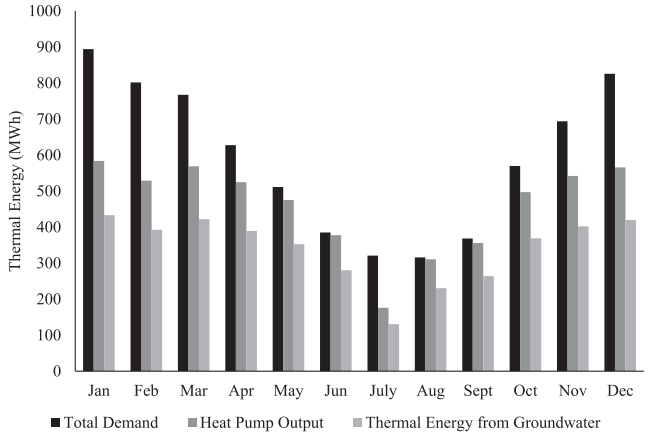

Fig. 6. Total design space heating demand, including DHW, heat pump output and thermal energy obtained from groundwater.

3. Numerical model development

The finite element subsurface flow and transport system (FEFLOW) has been chosen as a simulation tool to carry out groundwater modelling for this open-loop heat pump system. The software has the capability of simulating fluid flow, groundwater age, contaminant, and heat transport. The software can be used for 2D or 3D simulations; saturated, unsaturated or variably saturated media; and transient or steady-state conditions [33].

3.1. Model description

The model domain was created with dimensions of 1320 m × 844 m × 300 m (length × width × depth), which ensures that flow and heat transfer occurs inside the domain to eliminate edge effects. The locations of the boreholes and observation points are shown in Fig. 8. The depths of each well were assigned in the simulation using the multilayer well function in FEFLOW based on the information given in Fig. 3 and Table 1. A constant water injection temperature of 5 °C was assigned to each injection well, aligning with the planned design of the project. This temperature choice was determined based on an anticipated 8 °C decrease in groundwater temperature as it passes through the heat exchanger.

The domain was divided into six different layers/strata depending on the simplified geological formation of the site, as given in Table 3. This enables us to apply different parameters for different layers and observe the thermal effects in different layers. The topsoil/made ground, sand, and gravel were considered the first layer in the simulation. The second layer contains Thames Group. The third layer is Lambeth Group & Thanet Sand. The fourth layer is White Chalk Sub-Group. And the last layer is the Gault Clay. These layers were divided into many elements to define the hydraulic and thermal properties of different soil types.

The number of elements and nodes are 4,614,796 and 2337555, respectively. The observation points were located mainly at 80, 135, and 180 m bgl. Additionally, the observation points were placed at the well surface (i.e., 0 m radial distance), 0.5 and 1 m radial distances from the well surface to observe the temperature profile of the soil.

Observation points were placed at the surface of all wells at 80, 135 and 180 m bgl. They were also located between the wells to observe the interaction between them. Several observation points were placed around the wells to observe the vertical thermal distribution. The results were also obtained between the surface of each well and the model boundary, as shown in Fig. 8.

Several sensitivity analyses were carried out to choose the right element size (mesh spacing) (see Fig. 9). The domain was discretised using triangle mesh with a maximum element size of 20 m chosen at the farthest boundary, with the element size decreasing to about 0.11 m around the wells. Since element size significantly impacts computational time, maximum size with low impact on thermal plume delay was chosen.

Transient simulations were performed for fluid flow and heat transport. For a simulation time control, automatic time-step control with an initial time-step length of 0.001 days and a maximum time-step size of 10 days was set. Computational time was considered to be kept at its shortest when choosing these parameters.

3.2. Initial and boundary conditions

A steady-state 3D flow simulation was performed to calculate groundwater level and hydraulic gradient through the model domain (see Fig. 10). Initial hydraulic heads of 4.4 and 1.31 m were set at the west and east boundaries, respectively, based on water level measurement conducted at the site [28]. Hydraulic head distribution through the model was validated using the measured groundwater level data [28] just before the pumping test, and good agreement was found. The result taken from the steady-state simulation was used as an initial condition for transient simulations.

Diurnal temperature variations in the air do affect the temperature at the shallow earth's surface. However, these fluctuations are shown to be negligible after 10–15 m bgl [34]. Therefore, to simplify the modelling process, the effect due to the variation in air temperature has been neglected. Different ground temperatures were set according to ground temperature measurements conducted by Boon et al. [30] (see Fig. 11). Based on a planned 8 °C drop in the groundwater temperature across the heat exchanger, the minimum injection temperature corresponds to 5 °C. This temperature was assigned to the nodes, which denote the location of the injection wells.

In this study, the authors aimed to investigate the real case scenario where the heating demand fluctuates during the year, where borehole abstraction rates vary, and heat pumps modulate with weather compensation. To simulate this dynamic system behaviour, the injection and abstraction rates were set as time-varying using the time series

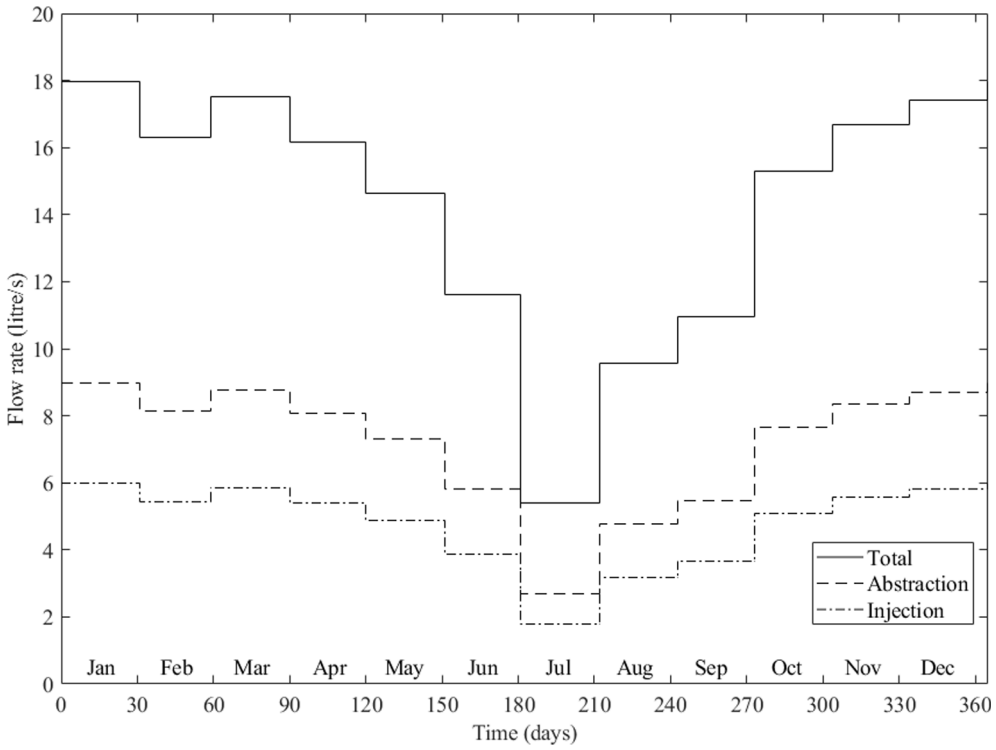

Fig. 7. Injection and abstraction flow rates per borehole type and total injection/abstraction rate used in the model simulations.

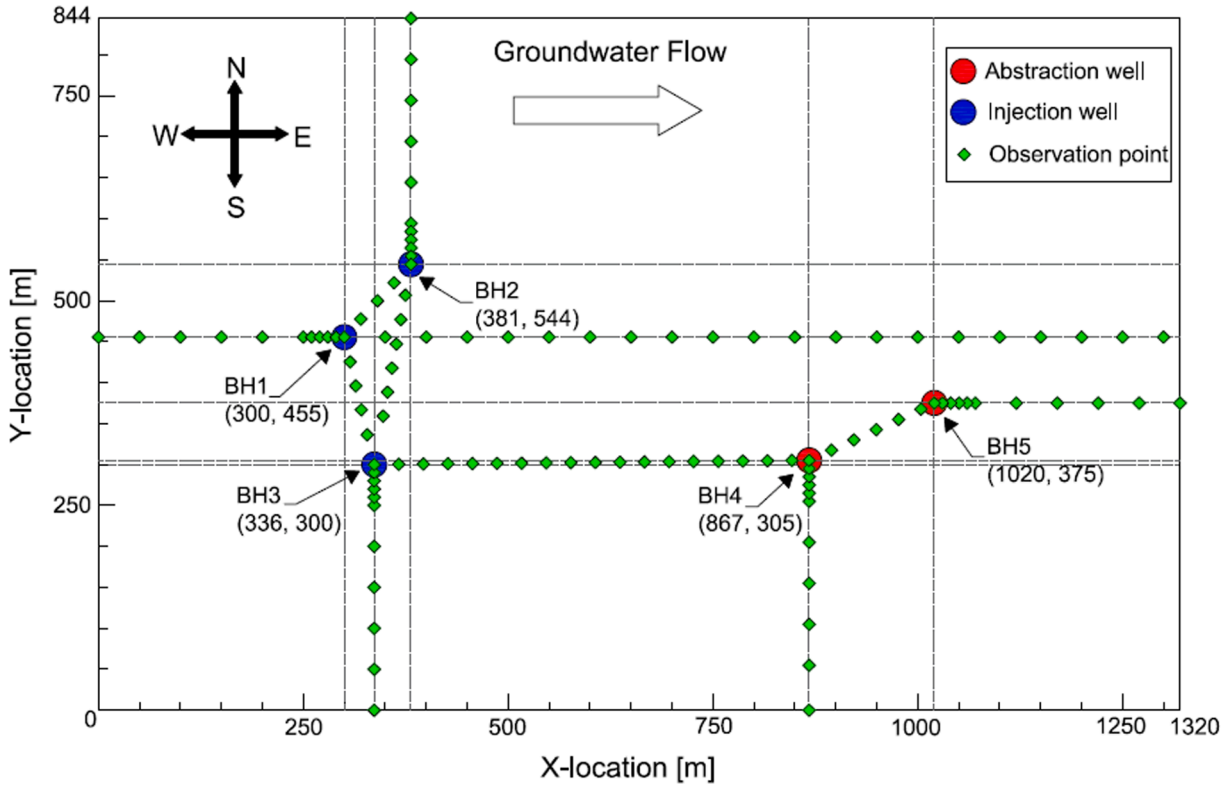

Fig. 8. Top view of the model domain with locations of wells and observation points.

function in FEFLOW, where the rates shown in Fig. 7 were applied.

3.3. Material parameters

Material properties for FEFLOW simulations have a significant impact on thermal plume development [9,10]. Therefore, it is important to consider all parameters used in the simulations to be able to achieve the most realistic results. In this study, the porosity [35] and thermal conductivity of the solids [20,21] were taken from the literature. The other properties, such as the volumetric heat capacity of the fluid and

Table 3
Simplified geological units used for the model [28].

Geological formation	Depth (m bgl)	Layer thickness (m)
Topsoil/Made Ground	0–0.8	0.8
Sands and Gravels	0.8–6	5.2
Thames Group	6–50	44
Lambeth Group & Thanet Sands	50–72	22
White Chalk Sub-Group	72–275	203
Gault Clay	275->300	Not proven

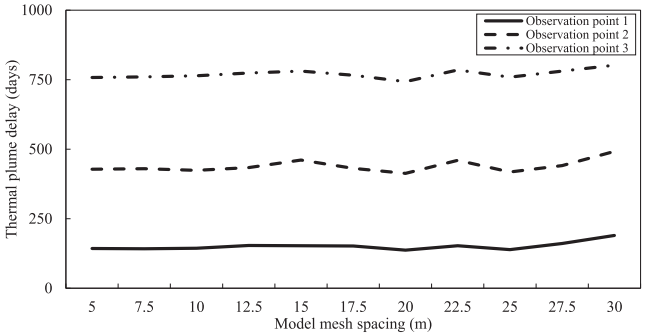

Fig. 9. Thermal plume delay at three observation points located downstream of the injection well.

solid, thermal conductivity of the fluid, and longitudinal and transverse dispersivity, were default values given in FEFLOW. The horizontal and vertical hydraulic conductivities of each layer were obtained from the validation analysis, which is explained in Section 4. Some of the material parameters used for the simulations are presented in Table 4.

3.4. Numerical simulation

A numerical modelling approach was used here to analyse the effect of the continuous heating operation on the aquifer and its impact on the system sustainability in a one-year operation for the considered case study. In this study, FEFLOW was used to carry out finite element modelling and simulations. This finite element code is based on mathematical principles of conservation of mass, momentum, and energy for the phases of solid, liquid, and gas, shown in equations (1–3), respectively.

Conservation of mass equation:

$$\frac{\partial}{\partial t}\left(\varepsilon_\alpha \rho^\alpha\right)+\frac{\partial}{\partial x_i}\left(\varepsilon_\alpha \rho^\alpha v_i^\alpha\right)=\varepsilon_\alpha \rho^\alpha Q_\rho^\alpha \tag{1}$$

Conservation of momentum equation:

$$v_i^\alpha+\frac{k_{ij}^\alpha}{\varepsilon_\alpha \mu^\alpha}\left(\frac{\partial p^\alpha}{\partial x_j}-\rho^\alpha g_j\right)=0 \tag{2}$$

Conservation of energy equation:

$$\frac{\partial}{\partial t}\left(\varepsilon_\alpha \rho^\alpha E^\alpha\right)+\frac{\partial}{\partial x_i}\left(\varepsilon_\alpha \rho^\alpha v_i^\alpha E^\alpha\right)+\frac{\partial}{\partial x_i}\left(j_{iT}^\alpha\right)=\varepsilon_\alpha \rho^\alpha Q_T^\alpha \tag{3}$$

where α is each phase, such as liquid water, vapour water, and solid particles; ε_α is the volume fraction of phase α $(0 \le \varepsilon_\alpha \le 1)$; ρ^α is the density of phase α [kg/m^3]; v_i^α is the velocity vector of phase α [m/s]; μ^α is the viscosity of phase α [kg/m-s]; k_{ij}^α is the permeability tensor of phase α [m^2]; Q_ρ^α and Q_T^α are the mass and heat supply of phase α, respectively; g_j is the gravity vector; p^α is the pressure of phase α; j_{iT}^α is the Fourierian heat flux vector of phase α; and E^α is the thermal energy of phase α [33].

The geological strata above and below the chalk aquifer have different characteristics and can significantly affect heat losses and gains. Therefore, the 3D approach was preferred even though the computational time is much longer and more complex than the 2D approach.

4. Results and discussion

4.1. Numerical model validation

A transient 3D simulation was run for 96 h to validate the numerical model based on field experimental data. The simulation duration was determined based on the test duration required to achieve an almost stabilised drawdown. The drawdown created by injection and

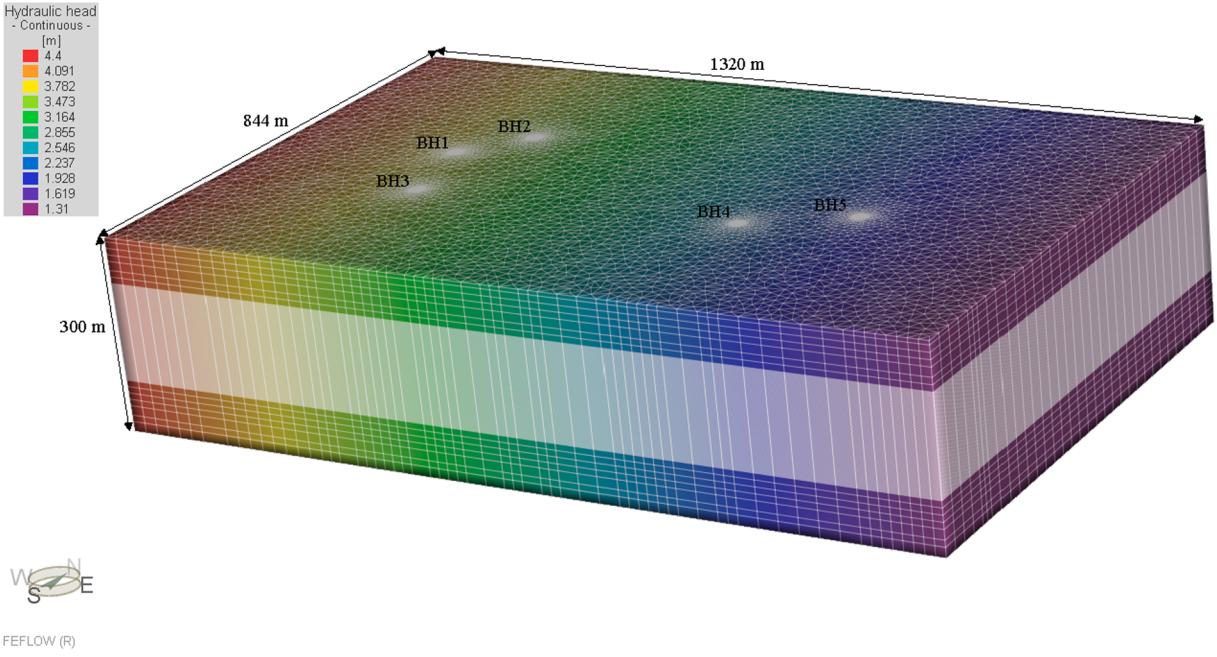

Fig. 10. Steady-state simulation result showing continuous hydraulic head (m aOD) through the model domain.

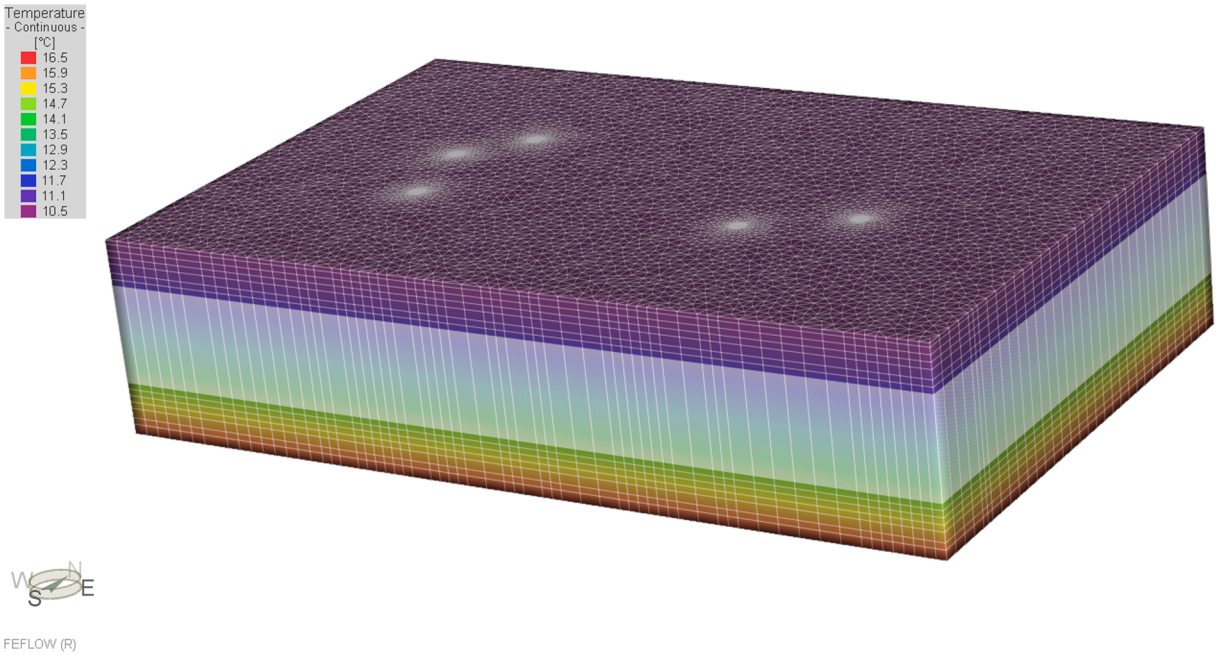

Fig. 11. Steady-state simulation result showing the undisturbed temperature distribution at different depths based on a local geothermal gradient of around 2.4 °C per 100 m [30].

Table 4
Material properties used in the simulation.

Layers	Ground depth (m)	Porosity	Volumetric heat capacity of fluid (MJ/m^3/K)	Volumetric heat capacity of solid (MJ/m^3/K)	Thermal conductivity of fluid (W/m.K)	Thermal conductivity of solid (W/m.K)	Longitudinal dispersivity (m)	Transverse dispersivity (m)
Layer 1	0–6	0.34	4.2	2.52	0.6	1.5	5	0.5
Layer 2	6–50							
Layer 3	50–72							
Layer 4 *	72–154					1.87		
Layer 4**	154–185					1.96		
Layer 4***	185–275					1.8		
Layer 5	275–300					1.5		

* Upper parts of the chalk, ** Middle parts of the chalk, *** Lower parts of the chalk.

abstraction in the field test was simulated. The abstraction and injection rates given for the simulation are 8 l/s and 5.3 l/s, respectively. The simulation results were compared with the field data, and a good match was found (see Fig. 12). It was observed that injection and abstraction create a drawdown at the wells, which may affect groundwater velocity.

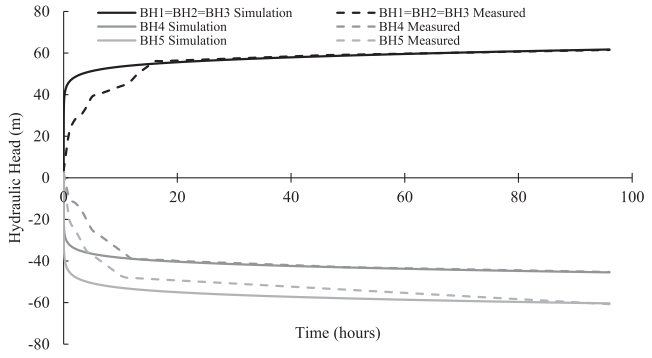

Fig. 12. Drawdown comparison between simulated and measured data at injection and abstraction wells for 96 h (4 days) [28].

As a result of the drawdown process, the groundwater may flow from injection wells to abstraction wells. This is not the best case for a GWHP system, as the groundwater temperature at the pumping wells can be affected. This situation increases the risk of thermal feedback, leading to a decrease in system efficiency and sustainability, particularly in the long term. Fig. 13 shows the hydraulic gradient around the wells. The water table is affected the most when the observation point is close to the wells, and the abstraction and injection have no effect on the water table after a radial distance of more than 100 m away from the wells.

The horizontal and vertical hydraulic conductivity significantly affect the drawdown and the thermal plume development. These values can be found in the literature in a range. The hydraulic conductivity of the soils may vary in the vertical direction as well as in the horizontal direction. Therefore, the validation study is used to predict hydraulic conductivity values for the different layers. The pumping test data shows that injection wells (BH1&2&3) and the first (BH4) and second abstraction well (BH5) have different drawdown results. Therefore, different horizontal hydraulic conductivity values were tried, calibrated, and applied to the different wells and their surroundings (Table 5). Depending on the site formation, the vertical hydraulic conductivity was predicted to be lower than the horizontal hydraulic conductivity. We assumed that the horizontal hydraulic conductivity is ten times higher

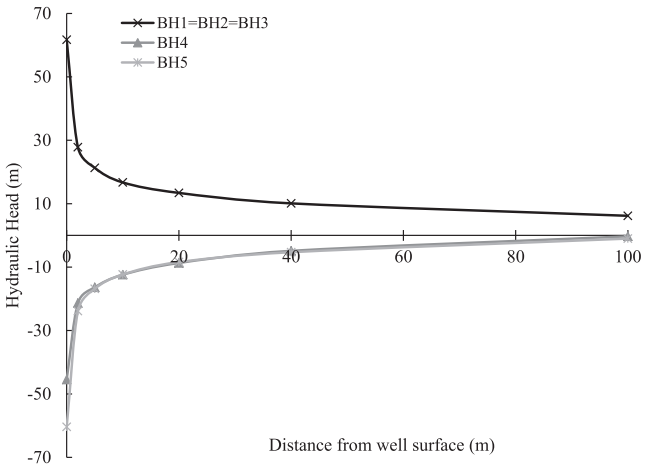

Fig. 13. Simulated hydraulic head distribution around the wells.

Table 5
Calibrated horizontal and vertical hydraulic conductivities used in the simulation.

Geological formation	Top level (m bgl)	Bottom level (m bgl)	Horizontal hydraulic conductivity (m/s)	Vertical hydraulic conductivity (m/s)
Topsoil/Made Ground, Sand and Gravels	0	6	5×10^{-4}	5×10^{-5}
Thames Group	6	50	5.8×10^{-11}	5.8×10^{-12}
Lambeth Group & Thanet Sands	50	72	2×10^{-8}	2×10^{-9}
White Chalk Sub-group	72	275	3.75×10^{-6}-8×10^{-9}	3.75×10^{-7}-8×10^{-10}
Gault Clay	275	300	8.3×10^{-12}	8.3×10^{-13}

than the vertical hydraulic conductivity.

White Chalk Sub-group has a wide range of hydraulic conductivity values due to the difference between chalk formations. The upper parts of the White Chalk have higher values than the lower ones because fractures tend to be more open and karstified immediately below the Palaeogene cover sediments.

4.2. Thermal energy calculations

The difference between undisturbed groundwater temperature and injection temperature is constant over a 1-year period, as the abstraction temperature is not affected by the thermal plume created by the operation.

The thermal energy gain from the groundwater can be calculated by the following equation:

$$\dot{Q} = \dot{m} C_{ave} \Delta T \tag{4}$$

where Q is the heat energy [kW], $\dot{m}$is the mass [kg/s], C_{ave} is the average specific heat calculated at the average temperature [kJ/kgK], and ΔT is the change in temperature [K] [36].

For the case study considered, Fig. 6 shows that the predicted total heating demand of the buildings is different for each month, and it is the highest in winter and lowest in summer. The highest heating demand is in January, with a demand of around 894 MWh, followed by the demand in December, with a quantity of about 826 MWh. The demand will be covered by the thermal energy extracted from groundwater with a rate of 48% and 51% in January and December, respectively. In February and March, the heating demand is relatively lower than in January and December, with a quantity of 802 and 767 MWh, respectively. 49% and 55% of the energy demand of the buildings is covered by the thermal energy gained from groundwater in February and March, respectively. The heating demand in November, April and October is 694, 627 and 570 MWh, of which 58%, 62% and 65% are supplied by geothermal energy, respectively.

In May, the total heating demand is 511 MWh, whilst it is around 385 MWh in June. The energy extracted from groundwater supplies 69% and 73% of the total demand in May and June, respectively. The total heating demand is around 320 and 315 MWh in July and August, respectively. The heat provided by the groundwater extraction is 73% in August, while it is comparably low in July with a rate of 41%, which could be a result of planned maintenance during this month.

As mentioned before, 75% of the total heating demand of the buildings is designed to be covered by the heat pump. However, 58% of the total demand will be covered by the energy gained from groundwater at the site. The difference will be the electrical input from the heat pump. The energy gain from the groundwater was calculated by considering the ΔT of 8 °C with abstraction and injection temperatures of 13 °C and 5 °C, respectively. The designed abstraction temperature was determined based on the results of the pump test conducted on the site [28]. The pump test showed that the groundwater temperature in the abstraction well increased from approximately 12.5 °C to 13.4 °C during the pumping test, possibly affected by the surface pipes warming in the sun. However, the simulation results show that the average temperature observed at the abstraction well remains at about 12.1 °C, which is the static temperature of the ground at the pumping level. The abstraction temperature obtained from the simulation is 0.9 °C lower than the actual designed value (see Fig. 14). Considering the abstraction temperature of 12.1 °C, ΔT equals to 7.1 °C. Fig. 14 shows that the temperature observed at the surface of the abstraction wells is constant during the operation as it is not affected by the water injection. Therefore, the thermal energy extraction from the groundwater in the simulation can also be calculated using Eq. (4).

Fig. 15 shows a comparison of the thermal energy gain between the actual designed system and the simulation results. The difference between them is 11.25% due to the difference in the abstraction temperature, and it can be covered by either increasing the monthly abstraction rate by 11.25% or decreasing the injection temperature to 4.1 °C. Increasing the abstraction rate might be a possible solution for low heating demand. For instance, during summer, the maximum abstraction rate is not reached; thus, the abstraction rate can be increased. However, it may not be possible during the peak loads, i.e., during winter, as it may exceed the maximum abstraction rate. Furthermore, in the case of decreasing the injection temperature to 4.1 °C, this would likely result in the risk of ground freezing. However, the UK

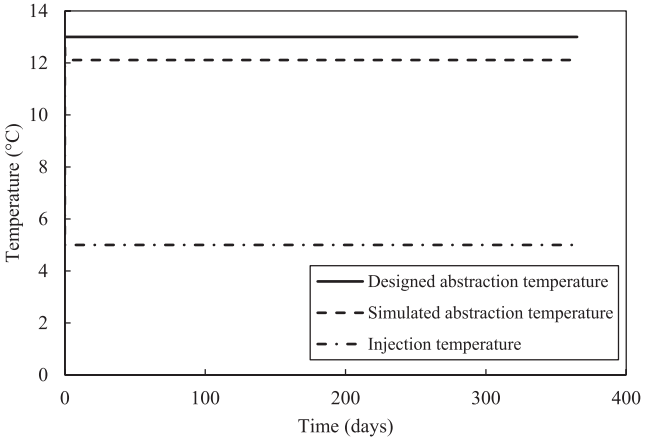

Fig. 14. Simulation results for abstraction and injection temperature during the operation.

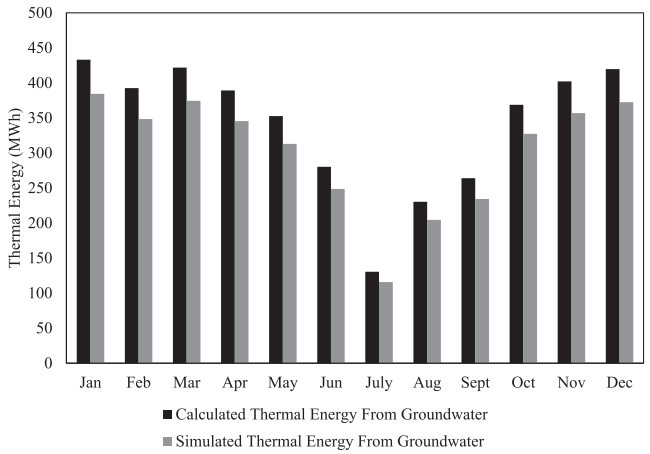

Fig. 15. Calculated and simulated results for the thermal energy gain from groundwater.

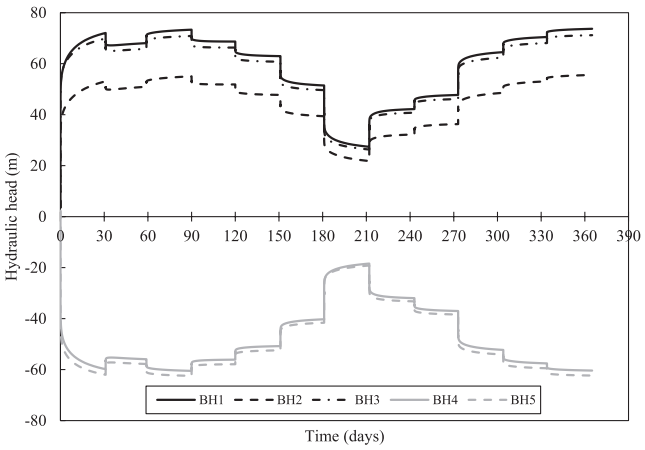

Fig. 16. Simulated water level variations in boreholes.

government's policy on groundwater usage [37] mandates that the difference between injection and abstraction temperatures must be less than 8 °C. Thus, the injection temperature was kept at 5 °C, thereby resulting in the difference between injection and abstraction temperature of 7.1 °C. This also ensures that the performance of the system is not jeopardised in the long term as a result of excessive heat solicitation.

The performance of the heat pumps is defined as the coefficient of performance, and it can be calculated by the following equation [6]:

$$COP = \frac{energyoutput}{energyinput} \tag{5}$$

The designed COP of the system is 3.91. However, the calculated COP value from the simulation results is around 3.47, which is 11.25% lower than the designed value. This decrease in COP is due to the difference between the designed and calculated abstraction temperature. This could be attributed to the conservative approach adopted in the modelling process, where additional energy gain from the sun, which could add to the system performance, was neglected. Additionally, the complexity of the site and its size makes it quite complicated in order to model the exact domain and in service heat loads explicitly. Thus, the thermal and hydraulic parameters adopted for the different layers are averaged to those found in literature and may vary both radially and axially.

4.3. Water level distribution

A transient 3D simulation was performed for a real case scenario for one year, where the validated model was used. The injection and abstraction rates shown in Fig. 7 were assigned. Fig. 16 shows the water level distribution in injection and abstraction wells. The water levels observed in the wells fluctuate throughout the year since the abstraction and injection rates differ each month. The maximum alteration was observed in December as the injection and abstraction rates are the highest this month, whilst the minimum change in water level can be seen in July as a result of the lowest abstraction and injection rates applied.

The elevations given in this section are in m aOD, and the top elevation of the wells (ground surface) is around 48 m aOD. The maximum water level observed in December is 73 m aOD (25 m above ground surface) due to the water injection at about 6.6 l/s in BH1. In December, the water level increases up to 55 and 71 m aOD in BH2 and BH3, respectively. Between the injection wells, BH2 is the least affected one. This can be due to the fact that BH2 goes deeper than the other two boreholes (see Table 1). BH1 is the one that was affected the most due to injection, and it can be attributed to its location as it is located between BH2 and BH3. And it is affected by water increases occurring in BH2 and BH3. In July, with the lowest injection rate of 1.8 l/s, the water levels at BH1, BH2 and BH3 are 27, 22 and 26 m aOD, respectively. As the maximum water level observed exceeds the ground surface in high-demand months, the water must be pressurised at a maximum quantity of around 2 bars in the field.

The water level observed in BH4 is slightly higher than in BH5. This can be attributed to the higher hydraulic conductivity value given for the BH5. This also shows that BH5 is slightly less productive than BH4. In December, the water level decreases up to −60 and −62 m aOD for BH4 and BH5, respectively, as a result of water abstraction at about 9 l/s per borehole. The lowest drawdown was observed in July, around −18.5 m aOD for BH4 and BH5 at a 2.7 l/s pumping rate per borehole. The highest drawdown is around 110 m bgl which is the elevation of the submersible pumps placed. Therefore, there might be an issue with abstraction if the water level drops below the elevation of the pumps.

4.4. Vertical thermal distribution

Fig. 17 shows the temperature distribution results with depth at the end of one year of simulation time. The results were obtained at the surface of the wells (i.e., 0 m radial distance), 0.5, 1 and 10 m radial distances from the well surface. It can be seen that the soil temperature at and around the wells decreases down to a maximum of 5 °C, which equals the injection temperature. The soil temperature drops significantly around the injection wells due to heat transfer via convection and conduction, especially at depths between 80 and 135 m bgl. This can be attributed to the coupled effect of higher hydraulic and thermal conductivity of the soil at a depth between 80 and 150 m bgl. That is where the upper part of the White Chalk aquifer lies and most thermal alteration occurs. Another reason for this is that all the wells have plane steel casing starting from the top of the well to 77 m bgl, which stops cold water from seeping into surrounding soil laterally.

The magnitude of the observed temperature in soil increases with the increase in distance to the injection well, which means that the observation points closer to injection wells have higher temperature changes. For instance, the observed temperature at 80 m bgl is 5 °C for the observation points at radial distances of 0, 0.5, and 1 m from the well surfaces. In comparison, it is 5.54 °C for the observation point located 10 m downstream from the injection wells.

Between the depths of 0 and 80 m bgl, the temperature observed at the injection wells (0 m) decreased to 5 °C. However, the effect of cold water injection decreased away from the injection wells (0.5, 1 and 10 m from the injection well) as a result of the steel casing from 0 to 77 m bgl. From 80 to 135 m bgl, the temperature decreased to 5 °C at the well surface and 0.5 and 1 m from the well surface. The temperature decrease is relatively lower at the observation point located 10 m from the well

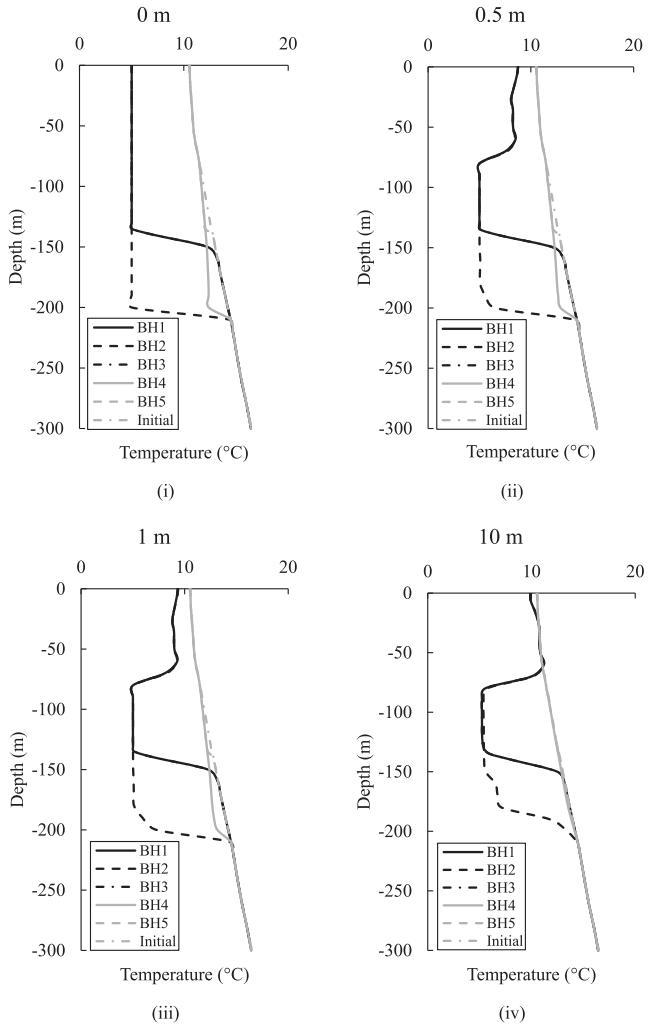

Fig. 17. Simulation results of temperature profiles obtained at (i) 0 m, (ii) 0.5 m, (iii) 1 m and (iv) 10 m away from the well surface.

surface, where the observed temperature is around 5.2 °C. Below 135 m depth, the observed temperature at BH1&3 suddenly increased to the initial soil temperature, meaning that the cold water injection has no impact below that level. This result can be attributed to the depth of the well screen that BH1&3 have. On the other hand, a significant temperature change was observed at BH2 up to 200 m bgl, which is the depth of BH2. Below 200 m, the temperature observed at BH2 increased quickly and reached the initial temperature of the soil.

BH4 and BH5 were not inside the affected zone as the maximum thermal plume dimension is around 50 m, and abstraction wells are located more than 530 m away from the injection wells. No effect related to injection temperature was observed. However, it should be noted that in long term operation, the thermal plume could extend toward the abstraction wells, potentially diminishing system efficiency. This is an ongoing study to predict the long-term impact and sustainability of the system. The temperatures at and around the abstraction wells show an increasing trend by the depth due to the initial temperature at the beginning of the simulation. On the other hand, there is an unexpected temperature decrease in BH4 at the depths between 150 and 200 m bgl, which is shown in the straight grey line in Fig. 17. This can be attributed to the interaction with the upper layers, which have relatively lower temperatures compared to the lower layers. The findings indicate an abstraction temperature of approximately 12.1 °C in both BH4 and BH5, considering the water extraction occurring at a depth of around 110 m bgl. This temperature falls below the intended abstraction temperature of 13 °C. As shown in Fig. 17, the maximum thermal alteration is observed at 135 m bgl. Therefore, this depth was chosen as a reference depth to better examine the thermally affected zone. Two other layers located at 80 and 180 m bgl were chosen to understand the thermal effects in chalk aquifers at different depths. These results are given in the following sections.

4.5. Thermal interaction between wells

Fig. 16 shows the results of the thermal interaction between injection wells, between abstraction wells and between injection and abstraction wells after one year of simulation time at the three aforementioned reference depths. Observation points closer to injection wells witnessed higher temperature change after one year, and the effect disappeared around the abstraction wells as the thermal plume did not reach the abstraction wells.

As shown in Fig. 18 (i) and (ii), the effect of injecting water in BH1 results in a temperature decrease of around 6.5 °C (from 11.5 °C to 5 °C) and 7.6 °C (from 12.6 °C to 5 °C) at 80 m bgl and 135 m bgl, respectively, at the surface of the well. The observed temperature of soil increases gradually to its original magnitude as moving away from the injection well. It increases with distance at a rate of about 1.7 °C and 1.6 °C per 10 m towards BH2 and BH3, respectively. The region of influence for BH1, BH2 and BH3 at 135 m bgl radially spans out to a distance of about 50 m, beyond which negligible to no temperature changes due to cold water injection into the wells were observed. Some thermal interactions exist between BH1 and BH2 as their influence regions/zones overlap slightly.

BH2 witnessed the same temperature decrease at the well surface at 80 and 135 m bgl. Additionally, the temperature at the well surface decreased from 13.7 °C to 5 °C at 180 m bgl. The thermal impact at 180

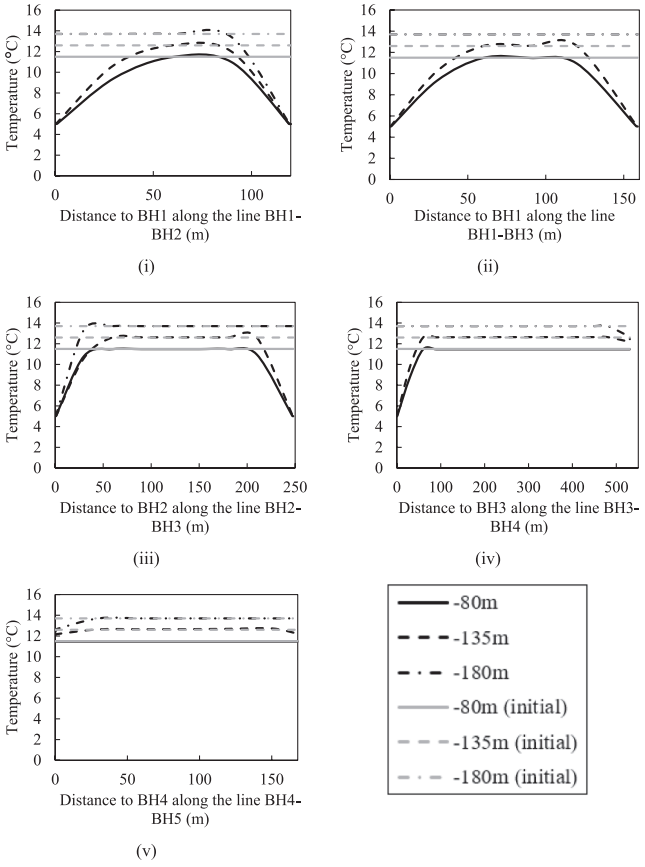

Fig. 18. Simulation results of temperature distribution between (i) BH1 and BH2, (ii) BH1 and BH3, (iii) BH3 and BH2, (iv) BH3 and BH4, and (v) BH5 and BH4 obtained at 80 m bgl, 135 m bgl and 180 m bgl.

m bgl was only observed for BH2 due to its depth which goes up to 200 m bgl. The rate of temperature increase is about 1.9 °C per 10 m towards BH1 and BH3 at 135 m bgl, whilst it is around 2.9 °C at 180 m bgl due to the low hydraulic and thermal conductivity values defined at this level.

The same temperature decrease was observed at the well surface of BH3. The rate of temperature increase in the direction towards BH1 and BH2 is about 1.6 °C, while it is around 1.5 °C in the direction towards BH4. The difference between the rates is negligible. However, it can be attributed to the effect of groundwater flow. The lowest increase rate was observed towards BH4 as it is the direction of the groundwater flow, which spreads cold water to a longer distance.

There are just negligible thermal effects around the abstraction wells, and that is due to the interaction between different layers where different initial temperatures were applied. A maximum of 0.5 °C drop in temperature was observed at and around the abstraction wells at 135 and 180 m bgl. No significant change was observed for the depth of 80 m bgl for BH4&5. However, if the thermal plume extends to the abstraction well, which is likely during long-term operation, BH4 and BH5 might experience a substantial temperature drop, leading to decreased efficiency and sustainability of the system.

4.6. Thermal interaction between wells and model boundary

The thermal interaction between wells and model boundary results are shown in Fig. 19 for 80, 135 and 180 m bgl. Each well is 300 m away from the closest boundary. As shown in Fig. 19 (i), the observed temperature at the well surface is around 5.1 °C at 80 m bgl for BH1 and BH3, with the temperature increasing with distance towards the model boundary at a rate of about 1.6 °C per 10 m. However, the observed temperature is 5.4 °C at the same depth for BH2 with an increasing rate of around 1.9 °C per 10 m towards the model boundary. The temperature at the well surface of injection wells was observed at about 5 °C at 135 m bgl, which is slightly lower than the temperature observed at 80 m bgl (see Fig. 19 (ii)). This can be due to different hydraulic and thermal conductivity values assigned to the layers above 80 m bgl and chalk. The temperature increase rate with a distance at 135 m bgl is slightly lower than at 80 m bgl. However, the abstraction wells and their surrounding areas witnessed a negligible change in temperature (up to 0.5 °C). As can be seen in Fig. 19 (iii), BH2 witnessed a temperature decrease of 8.7 °C (from 13.7 °C to 5 °C) at the well surface with an increasing rate of 2.8 °C per 10 m towards the model boundary, whilst other boreholes witnessed almost no change in temperature at 180 m bgl.

The maximum influence region for injection wells radially spans out to about 40 and 50 m at 80 and 135 m bgl, respectively, after which negligible temperature changes because of cold water injection were observed. Beyond 40 and 50 m radial distance from the surface of the wells, the temperature remained constant at the initial values which are 11.5 °C and 12.6 °C at 80 m bgl and 135 m bgl, respectively.

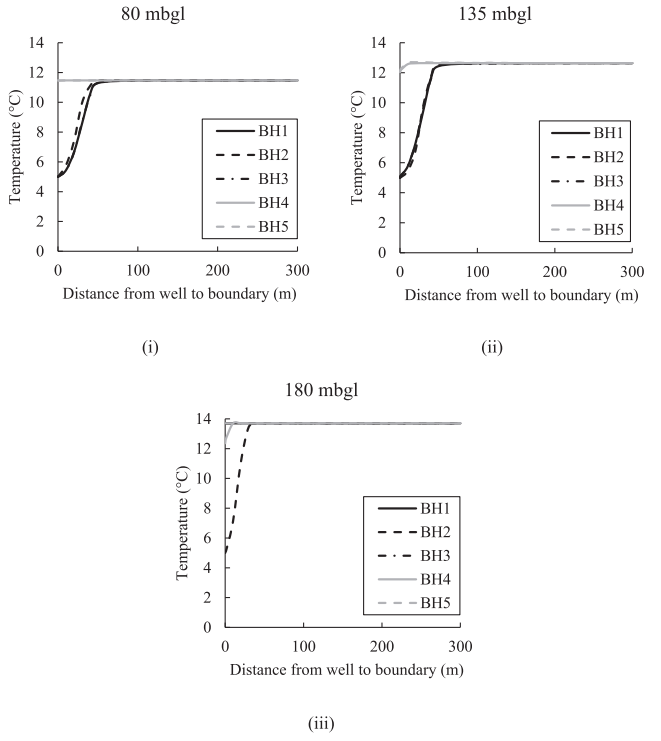

Fig. 19. Simulation results of thermal interaction between wells and model boundary at (i) 80 m bgl, (ii) 135 m bgl and (iii) 180 m bgl.

4.7. Temperature evolution

The results of temperature evolution versus time obtained at a depth of 80, 135, and 180 m bgl of BH1 are shown in Fig. 20. The results were obtained at a radial distance of 0, 0.5, 1, 5, 10, 20, 30, 40, 50, and 100 m from the surface of BH1. They show that a higher temperature drop was observed at the locations close to injection wells. However, this situation

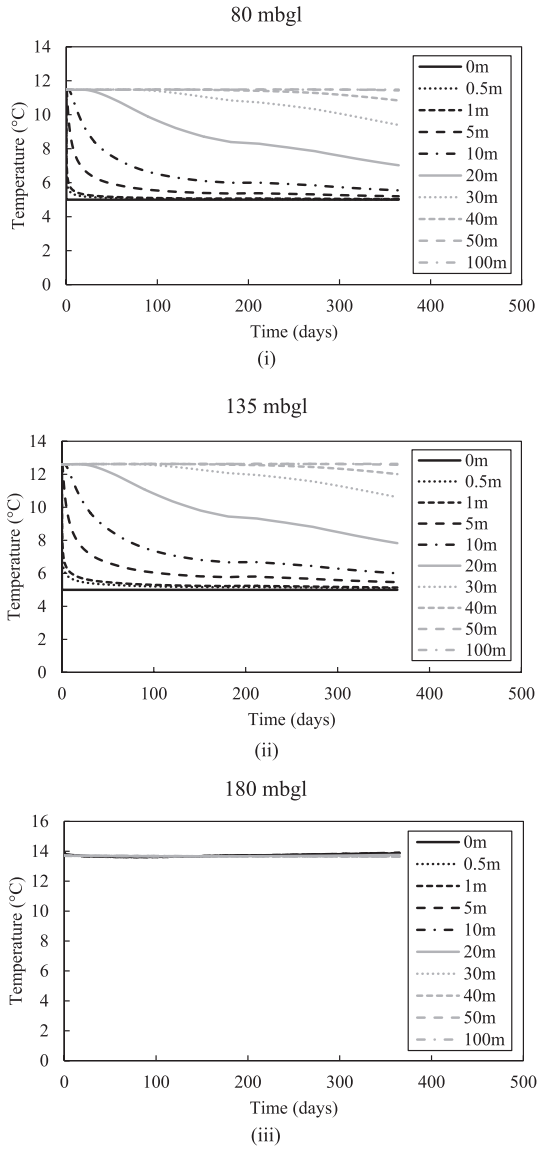

Fig. 20. Simulation results of thermal evolution in BH1 after one year operation at (i) 80 m bgl, (ii) 135 m bgl and (iii) 180 m bgl.

applies to depths of 80 and 135 m bgl. And a negligible temperature change was observed at 180 m bgl (see Fig. 20 (iii)). This can be attributed to the lower hydraulic and thermal conductivity of the soil in the lower parts of the chalk aquifer and shallower depth of BH1 (up to 135 m bgl).

The observed temperatures at 80 m bgl are slightly lower compared to 135 m bgl. This is because the initial temperature given is lower at 80 m bgl (see Fig. 5). It can be seen that the temperature went down drastically at the observation points located at a radial distance of 0, 0.5 and 1 m from the injection well surface until day 30, with an average temperature decrease of 0.17 °C per day. However, the decrease slowed after 30 days, and the temperature at these points reached around 5 °C at the end of the simulation, with an average temperature drop of 0.004 °C per day.

Fig. 20 (i) shows that at the end of the simulation, the observed temperature at a radial distance of 5 m, 10 m, 20 m and 30 m from the injection well surface is 5.2 °C, 5.5 °C, 7 °C and 9.4 °C with a temperature drop rate of 55%, 52%, 40% and 19%, respectively. It took almost 30 days and 100 days for the thermal plume to be observed at the observation points located at a radial distance of 20 and 30 m from the injection well surface, respectively. The furthest observation point affected by the water injection is 50 m away from the injection well surface at 80 m bgl. After that point, negligible changes were found.

Observation points located 0, 0.5, and 1 m away from the surface of the injection wells witnessed a sudden decrease in temperature at 135 m bgl. The temperature observed at the well surface decreased to 5 °C, which is around a 7.6 °C drop, considering the initial temperature of 12.6 °C, just after the injection started, and it remained constant until the end of the simulation. The temperature decrease is about 60% at the injection well surface. A sharp decrease in temperature was observed at the points located 0.5 and 1 m away from the injection well surface at 135 m bgl after around one day, and these are 6.3 °C and 5.5 °C, respectively. After 30 days, the temperature reached almost a steady-state condition. The temperature observed at these locations decreased to around 5.1 °C after one year of operation with a decrease rate of 60%.

As shown in Fig. 20 (ii), the influence of the temperature drop decreases with distance. The farthermost observation point affected by water injection is the point located 50 m downstream of the injection wells, after which negligible temperature changes were observed. This shows that the thermal plume dimension towards abstraction wells is around 50 m, which can be attributed to coupled heat transfer due to conduction and convection within the chalk. At the end of the simulation, the observed temperature at a radial distance of 5, 10, 20, 30 and 40 m from the injection well surface is 5.5 °C, 6 °C, 7.8 °C, 10.6 °C and 12 °C with a temperature decrease of 56%, 52%, 38%, 16% and 5%, respectively. The time lag that it took for the temperature change to be observed at these points located at a radial distance of 20, 30 and 40 m from the injection well surface is 30, 100 and 200 days, respectively.

The depth of 180 m bgl witnessed no changes in temperature, which can be attributed to low hydraulic and thermal conductivity values assigned to the lower parts of the chalk. It is also due to the depth of the well screen, which goes down to 135 m bgl for BH1.

5. Applicability of the current investigation

The findings of this study hold significant implications for the Colchester Northern Gateway Heat Network, providing valuable insight into the predicted performance and thermal behaviour of the GWHP system under continuous heating operation.

One of the key aspects explored in this study is the analysis of temperature changes within the soil using the design parameters. The research scrutinises both the overall temperature magnitude and the specific temperature distribution patterns. This analysis includes understanding the deviations in temperature concerning the initial conditions and identifying areas with maximum temperature variations. These insights not only provide a detailed understanding of how the system impacts the thermal characteristics of the soil but also shed light on potential hotspots or areas of concern.

The temperature distribution analysis aids in predicting the performance of the system throughout the year under consistent operating conditions. The research provides a comprehensive overview of the expected system performance, highlighting the heating capacities anticipated over the course of a year. This information is crucial for project planners and designers as it offers insight into the system's behaviour over extended periods, aiding informed decision-making during the operational phase.

The implications derived from the temperature and thermal performance analysis serve as a vital resource for project designers. By highlighting areas where the soil temperature experiences significant changes, designers can proactively account for these fluctuations during the system setup. This information becomes pivotal in refining the design parameters to ensure optimal performance and long-term sustainability. Moreover, the study acts as a foundation for future, more extended research initiatives. It serves as a precursor, guiding researchers towards specific areas of interest for in-depth, long-term studies, ensuring a robust understanding of the system behaviour over extended operational periods.

6. Conclusions

The main objective of this paper is to use a numerical approach to investigate the thermal impact of a district-scale GWHP operation where the groundwater is extracted from the UK chalk aquifer, considering a case study called Colchester Northern Gateway Heat Network in Essex, UK. This paper also aims to investigate the thermal plume developed by the heating operation and its effect on the system performance. The key findings are as follows:

- Abstraction and injection significantly impact the water level at and around the injection and abstraction wells, which creates a very high head difference of up to 122 m between the injection and abstraction wells compared to the initial head difference of about 1.4 m. It was thought that this could affect the groundwater flow during the operation. However, it was found that the effect of the head difference between injection and abstraction wells on groundwater flow is negligible. Furthermore, the drawdown created by groundwater abstraction may cause the water level to drop below the submersible pump and may affect the abstraction.
- The vertical thermal distribution mainly occurs in the upper parts of the chalk aquifer as a result of their higher hydraulic and thermal conductivity compared to the lower parts of the chalk. Therefore, the injection significantly affects the depths between 80 and 135 m bgl for BH1 and BH3 due to coupled convection via liquid and conduction via the solid soil skeleton. However, BH2 and its surrounding area were affected by cold water injection between 80 and 200 m bgl. This can be attributed to the different depths of the injection boreholes since the depth of BH1 and BH3 is 135 m bgl, while it is 200 m bgl for BH2.
- The interaction and heat transfer between the wells occur due to both conduction and convection and they become significant when the wells are closer to each other, i.e., BH1-BH2 and BH1-BH3.
- The modelling results show that the space heating operation creates a cold thermal plume, which develops mainly around the injection wells radially due to conduction and convection. The farthermost region to which the thermal plume reaches is the point located 50 m away from the injection well surface at 135 m bgl. The groundwater flow direction also has an impact on thermal plume development. However, it is negligible in this application as the groundwater flow velocity is slow.
- The geothermal thermal energy gain (thermal productivity) from the simulation results is 11.25% lower than the actual designed value, which is due to the difference between the designed and calculated

abstraction temperature. Nonetheless, the 11.25% difference in the energy gain can be compensated by either increasing the abstraction flow rate (which will result in higher drawdowns) or decreasing the injection temperature to 4.1 °C. The former may not be possible during the winter at peak loads as the water level may go below the level of the downhole pumps, and the latter may cause environmental impacts such as the risk of freezing.

- It can be concluded that in the first year of operation the thermal plume should not affect the abstraction temperature as the shortest distance between injection and abstraction wells is 530 m.
- The GWHP system, which has a heat pump working at a designed COP value of 3.91, established at this site can cover about 75% of the total heating demand of the buildings. However, the simulation results show that the COP is 11.25% lower than the designed value, and it is around 3.47, due to lower abstraction temperature found from the simulation results.
- Since a significant part of heating demand is covered by GWHP, the system enables us to produce thermal energy on a district scale for healthcare buildings, dwellings, and offices with very low GHG emissions.
- A conservative modelling approach was adopted in this study, and this may be site-specific. However, it provides a guide for designers and industry experts on what to anticipate during the design and installation of district-scale multi-well GWHP systems.

CRediT authorship contribution statement

Taha Sezer: Methodology, Software, Validation, Formal analysis, Investigation, Writing – original draft. **Abubakar Kawuwa Sani:** Writing – review & editing, Supervision. **Rao Martand Singh:** Writing – review & editing, Supervision. **Liang Cui:** Writing – review & editing, Supervision. **David P. Boon:** Resources, Writing – review & editing. **Michael Woods:** Resources, Writing – review & editing.

Declaration of Competing Interest

The authors declare that they have no known competing financial interests or personal relationships that could have appeared to influence the work reported in this paper.

Data availability

The data that has been used is confidential.

Acknowledgements

This research did not receive any specific grant from funding agencies in the public, commercial, or not-for-profit sectors. The authors would like to thank Colchester Amphora Energy for providing project data. The first author of this paper, Taha Sezer, is grateful for receiving the funding for his Ph.D. from the Ministry of National Education of Türkiye. David Boon publishes with permission of the executive director of the British Geological Survey.

References

[1] D. D'Agostino, B. Cuniberti, P. Bertoldi, Energy consumption and efficiency technology measures in European non-residential buildings, Energy Build 153 (Oct. 2017) 72–86, https://doi.org/10.1016/j.enbuild.2017.07.062.
[2] S. Buffa, M. Cozzini, M. D'Antoni, M. Baratieri, R. Fedrizzi, 5th generation district heating and cooling systems: A review of existing cases in Europe, Renew. Sustain. Energy Rev. (2019), https://doi.org/10.1016/j.rser.2018.12.059.
[3] D. Banks, An introduction to 'thermogeology' and the exploitation of ground source heat, Q. J. Eng. Geol. Hydrogeol. 42 (3) (2009) 283–293, https://doi.org/10.1144/1470-9236/08-077.
[4] M. Bloemendal, T. Olsthoorn, F. Boons, How to achieve optimal and sustainable use of the subsurface for Aquifer Thermal Energy Storage, Energy Policy 66 (2014) 104–114, https://doi.org/10.1016/j.enpol.2013.11.034.
[5] E. Milnes, P. Perrochet, Assessing the impact of thermal feedback and recycling in open-loop groundwater heat pump (GWHP) systems: a complementary design tool, Hydrogeol J 21 (2) (Sep. 2013) 505–514, https://doi.org/10.1007/s10040-012-0902-y.
[6] R.M. Singh, A.K. Sani, T. Amis, An overview of ground-source heat pump technology. Elsevier Inc., 2019. doi: 10.1016/b978-0-12-814104-5.00015-6.
[7] D. Banks, Thermogeological assessment of open-loop well-doublet schemes: A review and synthesis of analytical approaches, Hydrogeol J. 17 (5) (2009) 1149–1155, https://doi.org/10.1007/s10040-008-0427-6.
[8] G. Taddia, S. Lo Russo, V. Verda, Comparison between neural network and finite element models for the prediction of groundwater temperatures in heat pump (GWHP) systems, in: Engineering Geology for Society and Territory - Volume 6: Applied Geology for Major Engineering Projects, Springer International Publishing, 2015, pp. 255–258, https://doi.org/10.1007/978-3-319-09060-3_41.
[9] S. Lo Russo, L. Gnavi, E. Roccia, G. Taddia, V. Verda, Groundwater Heat Pump (GWHP) system modeling and Thermal Affected Zone (TAZ) prediction reliability: Influence of temporal variations in flow discharge and injection temperature, Geothermics, vol. 51, pp. 103–112, Jul. 2014, doi: 10.1016/j.geothermics.2013.10.008.
[10] S. Lo Russo, G. Taddia, V. Verda, Development of the thermally affected zone (TAZ) around a groundwater heat pump (GWHP) system: A sensitivity analysis, Geothermics, vol. 43, pp. 66–74, Jul. 2012, doi: 10.1016/j.geothermics.2012.02.001.
[11] A. Casasso, R. Sethi, Modelling thermal recycling occurring in groundwater heat pumps (GWHPs), Renew Energy 77 (May 2015) 86–93, https://doi.org/10.1016/j.renene.2014.12.003.
[12] Y. Nam, R. Ooka, Numerical simulation of ground heat and water transfer for groundwater heat pump system based on real-scale experiment, Energy Build 42 (1) (Jan. 2010) 69–75, https://doi.org/10.1016/j.enbuild.2009.07.012.
[13] A. Galgaro, M. Cultrera, Thermal short circuit on groundwater heat pump, Appl Therm Eng 57 (1–2) (Aug. 2013) 107–115, https://doi.org/10.1016/j.applthermaleng.2013.03.011.
[14] D.P. Boon, et al., Groundwater heat pump feasibility in shallow urban aquifers: Experience from Cardiff, UK, Sci. Total Environ. 697 (2019), https://doi.org/10.1016/j.scitotenv.2019.133847.
[15] W. Pophillat, G. Attard, P. Bayer, J. Hecht-Méndez, P. Blum, Analytical solutions for predicting thermal plumes of groundwater heat pump systems, Renew Energy 147 (2020) 2696–2707, https://doi.org/10.1016/j.renene.2018.07.148.
[16] S. Lo Russo, G. Taddia, G. Baccino, V. Verda, Different design scenarios related to an open loop groundwater heat pump in a large building: Impact on subsurface and primary energy consumption, Energy Build, vol. 43, no. 2–3, pp. 347–357, Feb. 2011, doi: 10.1016/j.enbuild.2010.09.026.
[17] S. Lo Russo, M.V. Civita, Open-loop groundwater heat pumps development for large buildings: A case study, Geothermics, vol. 38, no. 3, pp. 335–345, Sep. 2009, doi: 10.1016/j.geothermics.2008.12.009.
[18] A. Herbert, S. Arthur, G. Chillingworth, Thermal modelling of large scale exploitation of ground source energy in urban aquifers as a resource management tool, Appl Energy 109 (2013) 94–103, https://doi.org/10.1016/j.apenergy.2013.03.005.
[19] M. Gropius, Numerical groundwater flow and heat transport modelling of open-loop ground source heat systems in the London Chalk, Q. J. Eng. Geol. Hydrogeol. 43 (1) (Feb. 2010) 23–32, https://doi.org/10.1144/1470-9236/08-105.
[20] D. Birks, C. Adamson, M. G. Woods, G. Holmes, Evaluation of measures to improve the performance of an open loop ground source heat pump system in the chalk aquifer: a case study, Quart. J. Eng. Geol. Hydrogeol., vol. 55, no. 2, May 2022, doi: 10.1144/qjegh2021-074.
[21] S. Arthur, H.R. Streetly, S. Valley, M.J. Streetly, A.W. Herbert, Modelling large ground source cooling systems in the Chalk aquifer of central London, Q. J. Eng. Geol. Hydrogeol. 43 (3) (Aug. 2010) 289–306, https://doi.org/10.1144/1470-9236/09-039.
[22] J. Headon, D. Banks, A. Waters, V.K. Robinson, Regional distribution of ground temperature in the Chalk aquifer of London, UK, Q. J. Eng. Geol. Hydrogeol. (2009) 313–323, https://doi.org/10.1144/1470-9236/08-073.
[23] H.H. Thorsteinsson, J.W. Tester, Barriers and enablers to geothermal district heating system development in the United States, Energy Policy 38 (2) (Feb. 2010) 803–813, https://doi.org/10.1016/j.enpol.2009.10.025.
[24] M.A. Sayegh, P. Jadwiszczak, B.P. Axcell, E. Niemierka, K. Bryś, H. Jouhara, Heat pump placement, connection and operational modes in European district heating, Energy Build 166 (2018) 122–144, https://doi.org/10.1016/j.enbuild.2018.02.006.
[25] Amphora Energy | New energy choices for the people of Colchester. Accessed: Apr. 09, 2020. [Online]. Available: https://amphora-energy.co.uk/.
[26] Weather and climate change - Met Office. Accessed: Aug. 30, 2021. [Online]. Available: https://www.metoffice.gov.uk/.
[27] Google Earth. Accessed: May 03, 2022. [Online]. Available: https://earth.google.com/web/@51.92045418,0.90649483,48.68508512a,2311.01747961d,35y,0h,0t,0r.
[28] E. De-wit, Pumping Test Factual Report Project Name : Colchester Northern Gateway Heat Network Stage Gate 4 Client : Colchester Amphora Energy Ltd, 2020.
[29] Record details |Colchester and Brightlingsea.| BGS maps portal | OpenGeoscience | Our data | British Geological Survey (BGS). Accessed: Oct. 08, 2023. [Online]. Available: https://webapps.bgs.ac.uk/data/maps/maps.cfc?method=viewRecord&mapId=9680.

[30] D. P. Boon, A. Butcher, B. Townsend, Geological and Hydrogeological Investigations in the Colchester Northern Gateway Boreholes: February 2020 survey, no. February, 2020.
[31] D.T. Aldiss, The stratigraphical framework for the Palaeogene successions London Basin, UK, British Geol. Soc. (2012).
[32] G. Birks, D., Coutts, C. A., Younger, P. L., Parkin, Development of a groundwater heating and cooling scheme in a Permo-Triassic sandstone aquifer in South-West England and approach to managing risks - Enlighten: Publications, 2015. Accessed: Jul. 28, 2022. [Online]. Available: http://eprints.gla.ac.uk/116692/.
[33] Hans-Jörg G. Diersch, FEFLOW Finite Element Modeling of Flow, Mass and Heat Transport in Porous and Fractured Media.
[34] A.K. Sani, R.M. Singh, T. Amis, I. Cavarretta, A review on the performance of geothermal energy pile foundation, its design process and applications, Renew. Sustain. Energy Rev. 106 (February) (2019) 54–78, https://doi.org/10.1016/j.rser.2019.02.008.
[35] D.J. Allen, et al., The physical properties of major aquifers in England and Wales, British Geol. Survey Technical (1997) 312.
[36] Y.A.C., Y. Cengel, Heat Transfer: A Practical Approach With EES CD, p. 896, 2002.
[37] Environmental good practice guide for ground source heating and cooling, 2010.